Low-EMF Wireless Power Transfer Systems of Four-Winding Coils with Injected Reactance-Compensation Current as Active Shielding

Keita Furukawa, Keisuke Kusaka, and Jun-ichi Itoh
Department of Electrical, Electronics and Information Engineering,
Nagaoka University of Technology, NUT
Nagaoka, Niigata, Japan
archer_FK@stn.nagaokaut.ac.jp, kusaka@vos.nagaokaut.ac.jp, itoh@vos.nagaokaut.ac.jp

***Abstract*—This paper proposes and analyzes low-radiation noise wireless power transfer (WPT) systems with active shielding. Current flowing on the additional windings around the WPT coils is compensated with additional power supplies to cancel the magnetic field generated by the WPT coils. The current of the additional windings is controled with the additional power supplies to achieve zero magnetic field at rated power. The additional power supplies increase in the RMS current of the additional windings to inject reactance-compensation current. As a result, a transmission power of 1 kW and a reduction in radiation noise by 39.5 dB are achieved with the proposed active shielding. In addition, it is revealed that the transmission power with the proposed method is increased by the magnetic field reduction.**

Keywords—active shielding, multiple magnetic coupling, radiation noise, wireless power transfer

I. Introduction

Wireless power transfer (WPT) systems have been attracted as battery charging systems of electric vehicles (EVs) to avoid electric shocks for safety [1–4]. Large radiation noise is generated by the WPT coils when batteries on EVs are charged [1]. The radiation noise negatively affects electric devices or human bodies near the WPT system [1]. Thus, the radiation noise is limited by several regulations, such as the International Commission on Non-Ionizing Radiation Protection (ICNIRP) 2010 guidelines and International Special Committee on Radio Interference (CISPR) guidelines [5–8].

Many studies have been conducted on modulations, topologies of converters, and configurations of the WPT coils to reduce the magnetic field generated by the WPT coils [9–19]. Conductive plates are used to cancel the magnetic field in general [12, 14]. However, a reduction in the magnetic field with the conductive plates is small, and eddy current loss is generated on the conductive plates [14]. Resonant shielding has been proposed to reduce the magnetic field drastically [13, 15]. The resonant shielding uses resonant capacitors connected to the additional windings around the WPT coils to increase RMS current of the additional windings [13, 15]. However, the effective frequency band is limited by resonant frequency [13].

Active shielding has been proposed to solve the problems with the conductive plates and resonant shielding [14–19]. Additional windings (canceling windings), which are connected to additional power supplies or the main windings, are wound around the WPT coils [14–19]. The canceling windings cancel the magnetic field [14–19]. The advantage of the active shielding is that radiation noise is decreased significantly because the phase and RMS values of the current are controllable [14, 15, 18, 19]. However, the influence on the power transmission has not been discussed in detail. Moreover, a voltage or current rating of the additional power supplies has not been discussed.

This paper proposes a novel design method for a low-radiation-noise WPT system with the active shielding. The current of the canceling windings is designed with the operating current when the WPT system is operated with the short-circuited canceling windings. The RMS current of the canceling windings is increased with the additional power supplies such as capacitive loads to inject reactance-compensation current. Moreover, the influence of the electrical and magnetic characteristics is clarified in a simulation and experiment of the WPT system designed under the condition of the short-circuited canceling windings. The advantage of the proposed method is that the loss and capacity of the additional power supplies are smaller than those of converters connected to the main windings because the additional power supplies do not contribute to power transmission. In addition, the magnetic field is adjustable with the change of the RMS current of the canceling windings. As a result, the reduction effects and influence on the transmission power are revealed according to the injected current.

II. Active Shielding

A. Outline of Active Shielding

Figure 1 shows the schematic diagram of the active shielding. The WPT coils are constructed with the same two circular coils which the canceling windings (winding #2 or #4) are wound around the main windings (winding #1 or #3). The canceling windings are connected to the additional power supplies to compensate for the current of the canceling windings.

Magnetic field is generated by the current of the windings. The magnetic field is proportional to the current of the winding

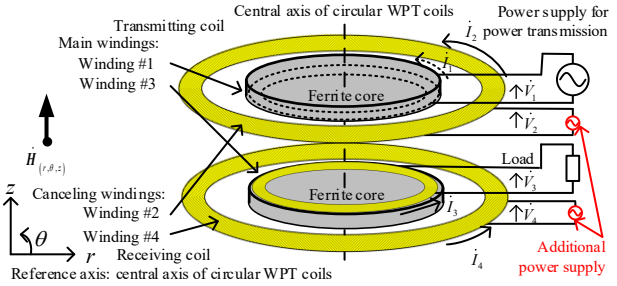

Fig. 1. WPT coils and active shielding.

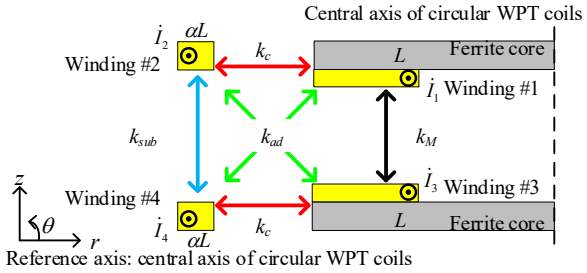

Fig. 2. Self-inductance and coupling coefficients of each winding.

when the magnetic field is the near field at the operational frequency of the WPT coils [16, 18, 19]. The magnetic field $\dot{\boldsymbol{H}}_{(r,\theta,z)}$ at any measurement point (r, θ, z) is given by

$$\dot{\boldsymbol{H}}_{(r,\theta,z)} = \sum_{m=1}^{4} \dot{\boldsymbol{H}}_{\boldsymbol{m}(r,\theta,z)} = \sum_{m=1}^{4} N_m \dot{I}_m \boldsymbol{h}_{\boldsymbol{m}(r,\theta,z)}$$

$$= \sum_{m=1}^{4} N_m \dot{I}_m \left(hr_m \boldsymbol{e}_r + h\theta_m \boldsymbol{e}_\theta + hz_m \boldsymbol{e}_z \right) \qquad (1)$$

where $\dot{\boldsymbol{H}}_{m\,(r,\,\theta,\,z)}$ is the magnetic field generated by the current I_m of the winding #m (m = 1, 2, 3, and 4), N_m is the number of turns of winding #m, $\boldsymbol{h}_{\boldsymbol{m}\,(r,\,\theta,\,z)}$ is the vectorial transfer function, hr_m, $h\theta_m$ and hz_m are the field components, and $\boldsymbol{e}_r$, $\boldsymbol{e}_\theta$, and $\boldsymbol{e}_z$ are the unit vectors of the cylindrical coordinate system.

The active shielding reduces $H_{(r,\,\theta,\,z)}$ with control of the current of the canceling windings. The advantage of the active shielding is that $H_{(r,\,\theta,\,z)}$ is decreased significantly. However, it is generally difficult to design the whole WPT system. The number of parameters, such as the current of the canceling windings and the size of the components of the WPT coils, is larger than a conventional two-winding WPT system. Moreover, the self-inductance and the coupling coefficient of the WPT coils from the view of the main windings are changed due to magnetic flux generated by the current of the canceling windings [13, 17]. The parameter variation of the WPT coils changes the electric characteristics of the WPT system, such as the transmission power and the whole efficiency. Thus, a design considering the parameter variation is necessary to achieve power transmission and effective reduction of the magnetic field.

B. Parameter Variation

This section analyzes the parameter variation of the WPT coils. The equivalent self-inductance L_{eq} and coupling coefficient k_{eq} from the view of the main windings are formulated when the canceling windings are shorted.

Figure 2 shows the cross-section of the WPT coils, the self-inductance L and αL of each winding, and the coupling coefficients k_c, k_M, k_{ad}, and k_{sub} between each pair of the windings. The transmitting coils and the receiving coils are the same configurations for simplification. The relationship between the current $\dot{I}_m$ and voltage $\dot{V}_m$ of the winding #m is given by (2) with the inductance matrix $\boldsymbol{L}$ when parasitic capacitance and resistance of the WPT coils is negligible.

$$\begin{bmatrix} \dot{V}_1 \\ \dot{V}_2 \\ \dot{V}_3 \\ \dot{V}_4 \end{bmatrix} = j\omega \boldsymbol{L} \begin{bmatrix} \dot{I}_1 \\ \dot{I}_2 \\ \dot{I}_3 \\ \dot{I}_4 \end{bmatrix} = j\omega \begin{bmatrix} L_{11} & L_{12} & L_{13} & L_{14} \\ L_{21} & L_{22} & L_{23} & L_{24} \\ L_{31} & L_{32} & L_{33} & L_{34} \\ L_{41} & L_{42} & L_{43} & L_{44} \end{bmatrix} \begin{bmatrix} \dot{I}_1 \\ \dot{I}_2 \\ \dot{I}_3 \\ \dot{I}_4 \end{bmatrix}$$

$$= j\omega L \begin{bmatrix} 1 & \sqrt{\alpha}k_c & k_M & \sqrt{\alpha}k_{ad} \\ \sqrt{\alpha}k_c & \alpha & \sqrt{\alpha}k_{ad} & \alpha k_{sub} \\ k_M & \sqrt{\alpha}k_{ad} & 1 & \sqrt{\alpha}k_c \\ \sqrt{\alpha}k_{ad} & \alpha k_{sub} & \sqrt{\alpha}k_c & \alpha \end{bmatrix} \begin{bmatrix} \dot{I}_1 \\ \dot{I}_2 \\ \dot{I}_3 \\ \dot{I}_4 \end{bmatrix} \qquad (2)$$

Here ω is the angular frequency, L_{mm} is the self-inductance of the winding #m, and L_{mn} ($m \neq n$, n = 1, 2, 3, and 4) is the mutual inductance between the winding #m and the winding #n. The diagonal component of $\boldsymbol{L}$ is the same.

The coupling coefficient k_{mn} is given by

$$k_{mn} = \frac{L_{mn}}{\sqrt{L_{mm} L_{nn}}} \qquad \left(|k_{mn}| < 1 \right) \qquad (3).$$

The coupling coefficient k_{mn} is determined by the configuration of the WPT coils. The number of turns of the windings does not change k_{mn}.

The self-inductance L is given by

$$L = \mathcal{P}_{main} N_{main}^{\ 2} \qquad (4),$$

where $\mathcal{P}_{main}$ and N_{main} are the permeance and the number of turns of the main windings, respectively.

The ratio α is given by

$$\alpha = \frac{\mathcal{P}_{cancel} N_{cancel}^{\ 2}}{\mathcal{P}_{main} N_{main}^{\ 2}} \qquad (5),$$

where $\mathcal{P}_{cancel}$ and N_{cancel} are the permeance and the number of turns of the canceling windings, respectively.

The equivalent parameters L_{eq} and k_{eq} are calculated with the

voltage condition ($\dot{V}_2 = \dot{V}_4 = 0$) and (2). The relationship of the voltage and current of the main windings are expressed in (6) when the canceling windings are short [17].

$$\begin{bmatrix} \dot{V}_1 \\ \dot{V}_3 \end{bmatrix} = j\omega \begin{bmatrix} L_{eq} & L_{eq}k_{eq} \\ L_{eq}k_{eq} & L_{eq} \end{bmatrix} \begin{bmatrix} \dot{I}_1 \\ \dot{I}_3 \end{bmatrix} \tag{6}$$

The equivalent self-inductance L_{eq} is shown in

$$L_{eq} = L\left\{1 - \frac{\left(k_{ad} + k_c\right)^2 - 2\left(1 + k_{sub}\right)k_c k_{ad}}{1 - {k_{sub}}^2}\right\} \tag{7}.$$

The equivalent coupling coefficient k_{eq} is shown in

$$k_{eq} = \frac{k_M\left(1 - {k_{sub}}^2\right) + k_{sub}\left({k_{ad}}^2 + {k_c}^2\right) - 2k_c k_{ad}}{\left(1 - {k_{sub}}^2\right) - \left({k_{ad}}^2 + {k_c}^2\right) + 2k_c k_{sub} k_{ad}} \tag{8}.$$

Equations (7) and (8) show that the current of the canceling windings decreases L_{eq} from L, and changes k_{eq} from k_M. Thus, the WPT system should be designed with L_{eq} and k_{eq} [17].

III. Proposed Method and Designing WPT Systems

A. Design Process used Proposed Method

Figure 3 shows the flowchart diagram of the proposed design method. The proposed method focuses on the processes to determine the current of the canceling windings after the process of making the WPT coils. The injected reactance-compensation current is determined with the phase and RMS of the current measured or calculated under the condition of power transmission when the canceling windings are short ($\dot{V}_2 = \dot{V}_4 = 0$). First, L_{eq} and k_{eq} are calculated with measured L, α, k_c, k_M, k_{ad}, and k_{sub} of the WPT coils. Second, the WPT system is designed with L_{eq} and k_{eq}. Next, the current phase and RMS of each winding are measured when the WPT system transmits rated power. Then, the injected reactance-compensation current is determined with the following equations.

The proposed method requires the WPT coils satisfing with (2) and a linear relationship between $\dot{\boldsymbol{H}}_{(r,\,\theta,\,z)}$ and $\dot{I}_m$. In particular, $H_{(r,\,\theta,\,z)}$ is reduced by the WPT coils with windings of high-quality factor significantly. The proposed method is useful to estimate whether the fundamental harmonics component of the magnetic field satisfies regulations of CISPR and ICNIRP guidelines.

B. Injected Reactance-compensate Current of Canceling Windings

This section describes how to decide the injected reactance-compensate current in the box of red dashed enclosing line in Fig. 3. The magnetic field $\dot{H}$ on the horizontal plane through at the center of the gap of the WPT coils. The z-axis component $\dot{H}_z$ and r-axis component $\dot{H}_r$ of $\dot{H}$ are

$$\begin{bmatrix} \dot{H}_z \\ \dot{H}_r \end{bmatrix} = \begin{bmatrix} hz_1N_1 & hz_2N_2 & hz_3N_3 & hz_4N_4 \\ hr_1N_1 & hr_2N_2 & hr_3N_3 & hr_4N_4 \end{bmatrix} \begin{bmatrix} \dot{I}_1 \\ \dot{I}_2 \\ \dot{I}_3 \\ \dot{I}_4 \end{bmatrix}$$

$$= \begin{bmatrix} hz_{main}N_{main}\left(\dot{I}_1 + \dot{I}_3\right) + hz_{cancel}N_{cancel}\left(\dot{I}_2 + \dot{I}_4\right) \\ hr_{main}N_{main}\left(\dot{I}_1 - \dot{I}_3\right) + hr_{cancel}N_{cancel}\left(\dot{I}_2 - \dot{I}_4\right) \end{bmatrix} \tag{9},$$

where N_{main} is the number of turns of the main windings, N_{cancel} is the number of turns of the main windings, hz_{main} and hr_{main} are the field components of the main windings, and hz_{cancel} and hr_{cancel} are the field components of the canceling windings because of the symmetry of the WPT coils in Fig. 2.

When the canceling windings are short, the components of $\dot{H}$ are expressed by

$$\begin{bmatrix} \dot{H}_z \\ \dot{H}_r \end{bmatrix} = \begin{bmatrix} \left(hz_{main} - hz_{cancel}\sqrt{\frac{\mathcal{P}_{main}}{\mathcal{P}_{cancel}}}\frac{k_c + k_{ad}}{1 + k_{sub}}\right)N_{main}\left(\dot{I}_1 + \dot{I}_3\right) \\ \left(hr_{main} - hr_{cancel}\sqrt{\frac{\mathcal{P}_{main}}{\mathcal{P}_{cancel}}}\frac{k_c - k_{ad}}{1 - k_{sub}}\right)N_{main}\left(\dot{I}_1 - \dot{I}_3\right) \end{bmatrix} \tag{10}.$$

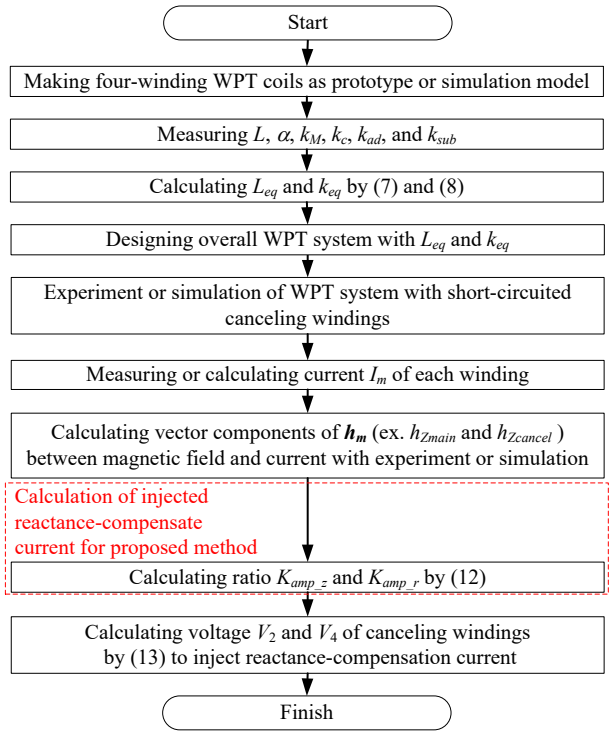

Fig. 3. Flowchart diagram of design processes include proposed method.

Equations (10) shows that the magnetomotive force of the canceling windings is the opposite phase to the magnetomotive force of the main windings. The number N_{cancel} is not related to H. The z-axis component H_z is zero when the item of hz_{main} is equal to the item of hz_{cancel}. However, H_z is not reduced enough with the short-circuited canceling windings because the item of hz_{cancel} is generally smaller than the item of hz_{main}. Reducing H_r is also the same mechanism. The proposed method increases the current RMS of the canceling windings in phase with the additional power supplies to reduce H.

Ratio K_{amp} of the current RMS is given by

$$K_{amp} = \left| \frac{\dot{I}_{2a}}{\dot{I}_{2s}} \right| = \left| \frac{\dot{I}_{4a}}{\dot{I}_{4s}} \right| \tag{11}$$

where $\dot{I}_{2s}$ and $\dot{I}_{4s}$ are the currents of windings #2 and #4 when the canceling windings are short, respectively, and $\dot{I}_{2a}$ and $\dot{I}_{4a}$ are the currents of windings #2 and #4 with the active shielding, respectively.

When the variations of $\dot{I}_1$ and $\dot{I}_3$ are negligible with the proposed method, zero H_r or H_z are achieved with proper K_{amp}. The ratio K_{amp_z} and K_{amp_r}, which achieve zero H_r and H_z, respectively, are shown in

$$\begin{cases} K_{amp\_z} \approx \sqrt{\dfrac{\mathcal{P}_{cancel}}{\mathcal{P}_{main}}} \dfrac{hz_{main}\left(1+k_{sub}\right)}{hz_{cancel}\left(k_c+k_{ad}\right)} \\ K_{amp\_r} \approx \sqrt{\dfrac{\mathcal{P}_{cancel}}{\mathcal{P}_{main}}} \dfrac{hr_{main}\left(1-k_{sub}\right)}{hr_{cancel}\left(k_c-k_{ad}\right)} \end{cases} \tag{12}$$

The ratio K_{amp_z} and K_{amp_r} are also evaluation criteria of the configuration of the WPT coils focused on H; the WPT coils with K_{amp_z} and K_{amp_r} of around one should be designed. Large

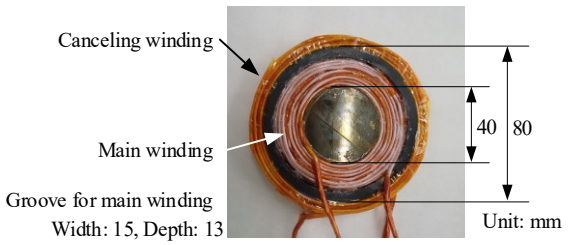

(a) Top view of transmitting coil.

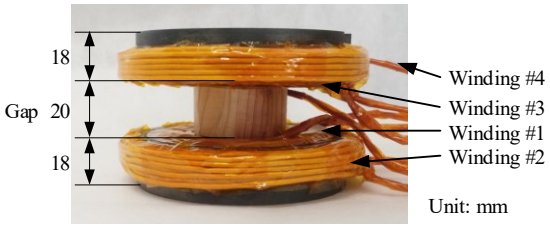

(b) Side view of overall WPT coils.

Fig. 4. Prototype of WPT coils.

K_{amp_z} or K_{amp_r} requires the large apparent power of the additional power supplies to cancel H because the volume and loss of a power supply become larger as the larger capacity in general. In particular, the additional power supplies are not needed to achieve zero H at $K_{amp\_z} = K_{amp\_r} = 1$.

The voltage $\dot{V}_2$ and $\dot{V}_4$ of winding #2 and #4 are shown in

$$\begin{bmatrix} \dot{V}_2 \\ \dot{V}_4 \end{bmatrix} = j\omega\alpha L\left(K_{amp}-1\right)\begin{bmatrix} 1 & k_{sub} \\ k_{sub} & 1 \end{bmatrix}\begin{bmatrix} \dot{I}_{2s} \\ \dot{I}_{4s} \end{bmatrix} \tag{13}$$

The imaginary equivalent impedance $\dot{Z}_{2a}$ and $\dot{Z}_{4a}$ of the additional power supplies are shown in

$$\begin{cases} \dot{Z}_{2a} = -\dfrac{\dot{V}_2}{\dot{I}_{2a}} = -j\omega\alpha L\left(1+k_{sub}\dfrac{\dot{I}_{4s}}{\dot{I}_{2s}}\right)\dfrac{K_{amp}-1}{K_{amp}} \\ \dot{Z}_{4a} = -\dfrac{\dot{V}_4}{\dot{I}_{4a}} = -j\omega\alpha L\left(1+k_{sub}\dfrac{\dot{I}_{2s}}{\dot{I}_{4s}}\right)\dfrac{K_{amp}-1}{K_{amp}} \end{cases} \tag{14}$$

Negative inductance is dominant in $\dot{Z}_{2a}$ and $\dot{Z}_{4a}$ because active power for k_{sub} is much smaller than reactive power of self-inductance in general WPT systems ($|k_{sub}| << 1$). The additional power supplies contribute to not the power transmission but the reduction of the magnetic field around the WPT coils.

IV. Experiment and Analysis with Prototype

A. Equivalent Values L_{eq} and k_{eq} of WPT Coils

Figure 4 shows the prototype of the WPT coils. The prototype is made as the miniature model for WPT coils for the battery charger in order to evaluate the proposed method. The pot cores are made with ferrite (TDK, PC40). The main winding is wound into the groove. The canceling winding is wound on the outside of the pot core. The gap between the transmitting coil and the receiving coil is 20 mm. The number of turns N_{cancel} is 20 turns to increase the quality factor of the canceling windings.

Table I shows the parameters of the prototype. The inductance, ESR, and coupling coefficients are measured with the LCR meter (HIOKI, 3532-50). Measured and calculated L_{eq} and k_{eq} are also shown in Table I. The validity of (7) and (8) is confirmed from an error of less than 0.5%.

B. Designing Circuit

Figure 5 shows the experiment circuit as the miniature model of the WPT systems. Table II shows the experiment condition with the experiment circuit. The input DC voltage V_{in} is 300 V, the operational frequency f_{sw} is 83.3 kHz, and the rated output power P_n is 1 kW as the miniature model. The experiment circuit is operated as the conventinal WPT system when the canceling windings are open ($I_2 = I_4 = 0$). Whereas, the experiment circuit is operated with the active sheildng when the canceling windings are short ($V_2 = V_4 = 0$) or connected to the additional power supplies ($K_{amp} \neq 1$). The operational frequency f_{sw}, V_{in} and the output DC voltage V_{out} refer to WPT battery charging systems

for EVs. Output DC voltages V_{out} of 390 V and 295 V are adjusted at $I_2 = I_4 = 0$ and $V_2 = V_4 = 0$ to transmit P_n, respectively. Bipolar power supplies are used as the additional power supplies.

The resonant capacitors C_{s1} and C_{s2} are connected to the main windings in serial to improve the power factor. The capacitance of C_{s1} and C_{s2} is given by

$$C_{s1} = C_{s2} = \frac{1}{\omega^2 L_{eq}} \tag{15}$$

from the resonant condition.

TABLE I. ELECTRIC AND MAGNETIC PARAMETERS OF PROTOTYPE

Parameter		Value
Self-inductance of main windings L		580 μH
Inductance ratio α		0.187
Coupling coefficient k_M		0.275
Coupling coefficient k_c		0.229
Coupling coefficient k_{ad}		0.185
Coupling coefficient k_{sub}		0.267
ESR of main windings r_{main}		1.03 Ω
ESR of canceling windings r_{cancel}		0.192 Ω
Number of turns of main windings N_{main}		51 turn
Number of turns of canceling windings N_{cancel}		20 turn
Permeance of main windings $\mathcal{P}_{main}$		2.23×10^{-7} H
Permeance of canceling windings $\mathcal{P}_{cancel}$		2.71×10^{-7} H
Equivalent self-inductance L_{eq}	Measured	537 μH
	Calculated	540 μH
	Error	0.5%
Equivalent coupling coefficient k_{eq}	Measured	0.224
	Calculated	0.224
	Error	< 0.2%

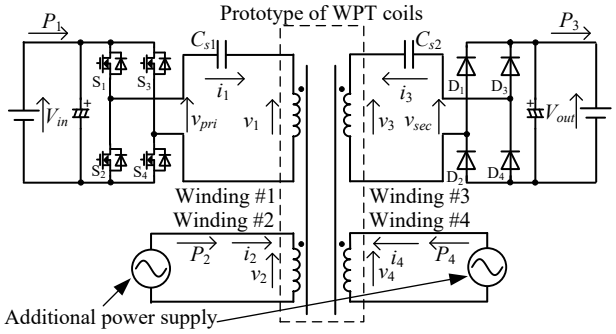

Fig. 5. Experiment circuit.

TABLE II. EXPERIMENT CONDITIONS

	Symbol	Value / model number	
Input DC voltage	V_{in}	300	V
Output DC voltage	V_{out}	295	V
		Open ($I_2 = I_4 = 0$): 390	V
Rated output power	P_n	1	kW
Switching frequency	f_{sw}	83.3	kHz
Angular frequency	ω	5.24×10^5	rad/s
Dead time	T_{dead}	250	ns
Resonant capacitors	C_{s1}, C_{s2}	6.30	nF
		Open ($I_2 = I_4 = 0$): 6.69	nF
MOSFETs	$S_1 - S_4$	SCH2080KEC (ROHM)	
Diodes	$D_1 - D_4$	SCS220AE (ROHM)	

C. Simulation of Magnetic Field with Proposed Method

In this section, H is estimated with electromagnetic field simulation (JSOL, JMAG-Designer) when the proposed method is applied to the experiment circuit.

Figure 6 shows the simulation model as the prototype and the measurement point. Table III shows $\dot{I}_m$, $\boldsymbol{h_m}$, K_{amp_z} and K_{amp_r}. The measurement point is at a horizontal distance of 50 cm from the center of the gap as the representative. The standard current $\dot{I}_m$ is the measured values from the experiment when the canceling windings are shorted.

Figure 7 shows H_z, H_r, and H when K_{amp} and the phase difference $\Delta\theta$ of $\dot{I}_{2s}$ and $\dot{I}_{4s}$ are changed. The magnetic field H_z and H reach a minimum at K_{amp_z} and $\Delta\theta = 0$ deg. Whereas, H_r reaches a minimum at a K_{amp} of 1.00 and $\Delta\theta = 10$ deg. The error between $K_{amp} = 1.00$ and K_{amp_r} occurs due to dimensional error. In addition, H approaches to H_z because $|hz_{main}|$ and $|hz_{cancel}|$ are much larger than hr_{main} and hr_{cancel} at the measurement point.

Figure 8 shows the distribution of the magnetic field around the simulation model of the prototype. The current $\dot{I}_m$ ($I_1 = 3.91$ A, $\dot{I}_2 = 0$ A, $\dot{I}_3 = 2.80\ e^{-j93.6°}$ A, and $\dot{I}_4 = 0$ A) in Fig. 7 (a) with the open canceling windings are measured with the experiment. The magnetic field is decreased by approximately 40 dB with the proposed method not only at the measurement point but also at a distance from the simulation model of the prototype.

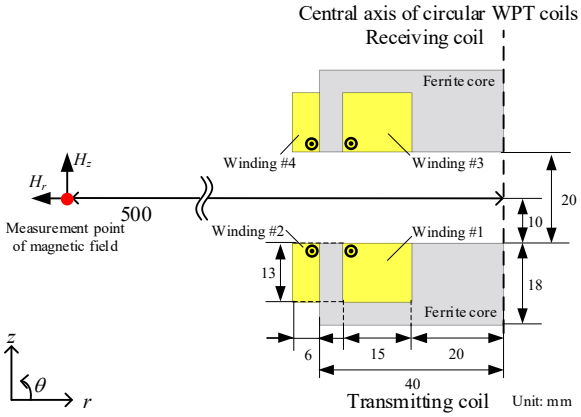

Fig. 6. Simulation model and measurement point.

TABLE III. VECTORAL TRANSFER FUNCTIONS AND CONDITION

Parameter	Value
Current $\dot{I}_1$ of winding #1	3.96 A
Current $\dot{I}_{2s}$ of winding #2	$2.10K_{amp}\ e^{j(144+\Delta\theta)°}$ A
Current $\dot{I}_3$ of winding #3	$3.75\ e^{-j92.3°}$ A
Current $\dot{I}_{4s}$ of winding #4	$2.00K_{amp}\ e^{j(126+\Delta\theta)°}$ A
Vectoral transfer function $\boldsymbol{h_1}$ of winding #1	$hr_{main}\boldsymbol{e_r} + hz_{main}\boldsymbol{e_z}$
Vectoral transfer function $\boldsymbol{h_2}$ of winding #2	$hr_{cancel}\boldsymbol{e_r} + hz_{cancel}\boldsymbol{e_z}$
Vectoral transfer function $\boldsymbol{h_3}$ of winding #3	$-hr_{main}\boldsymbol{e_r} + hz_{main}\boldsymbol{e_z}$
Vectoral transfer function $\boldsymbol{h_4}$ of winding #4	$-hr_{cancel}\boldsymbol{e_r} + hz_{cancel}\boldsymbol{e_z}$
Vector component hz_{main}	-2.43×10^{-3} /m
Vector component hz_{cancel}	-6.70×10^{-3} /m
Ratio K_{amp_z}	1.22
Vector component hr_{main}	3.04×10^{-5} /m
Vector component hr_{cancel}	6.30×10^{-4} /m
Ratio K_{amp_r}	0.886

*The measurement point of the magnetic field is shown in Fig. 5

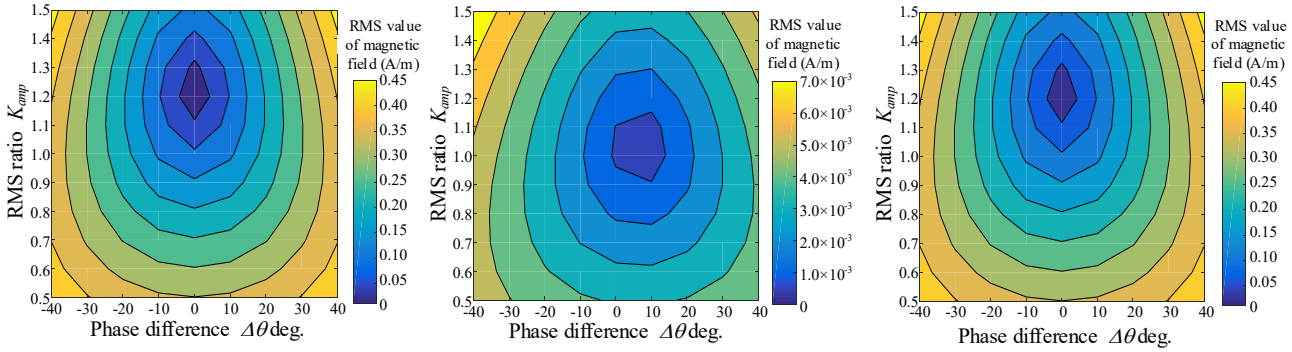

(a) Z-axis component H_z. (b) R-axis component H_r. (c) Magnetic field H.

Fig. 7. Estimation of Magnetic field with electromagnetic field simulation.

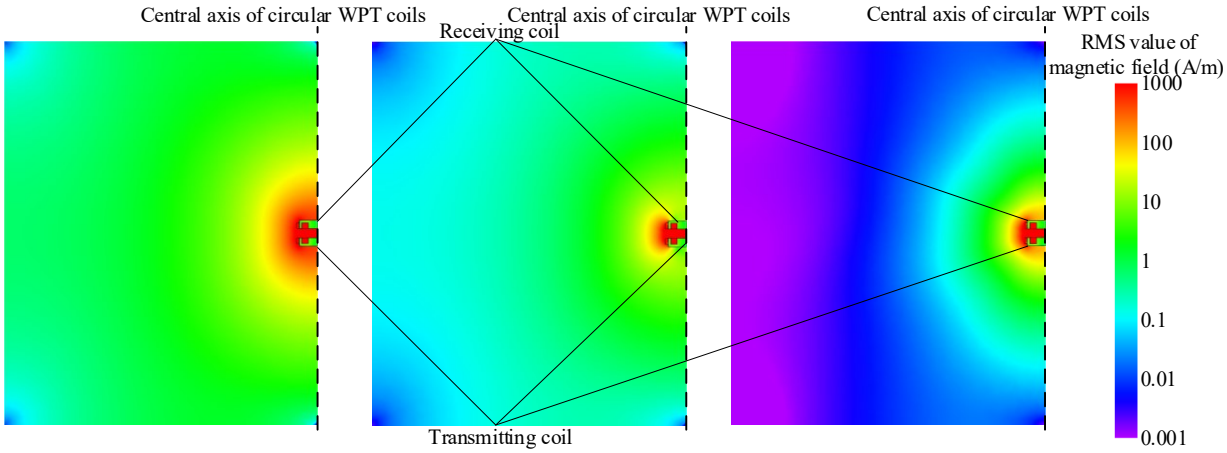

(a) Open canceling windings. (b) K_{amp} = 1.0 and $\Delta\theta$ = 0 deg. (c) Minimum H (K_{amp} = 1.22, $\Delta\theta$ = 0 deg.).

Fig. 8. Magnetic field around WPT coils.

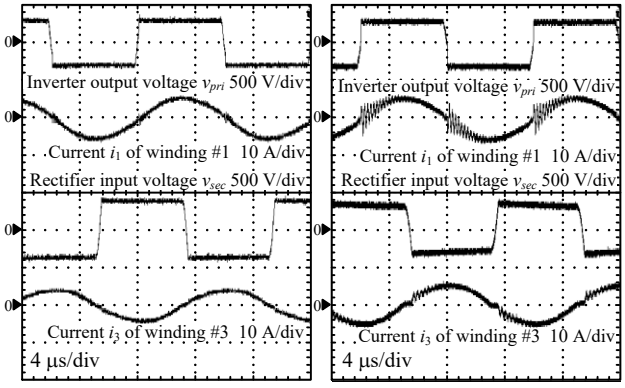

(a) Open canceling windings. (b) Short-circuited canceling windings.

Fig. 9. Operating waveforms.

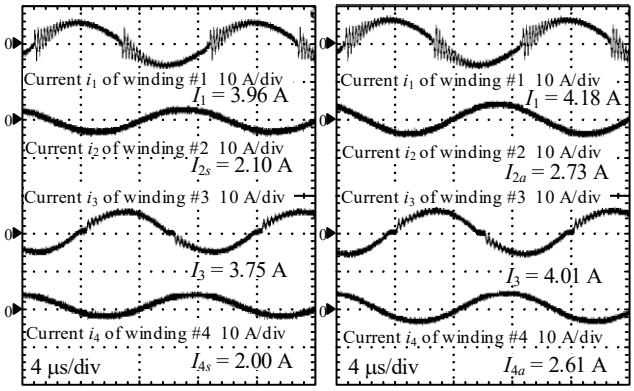

(a) Ratio K_{amp} = 1.00. (b) Ratio K_{amp} = 1.30.

Fig. 10. Current of each winding.

D. Operational Waveforms

Figure 9 shows the voltage and current v_{pri}, v_{sec}, i_1, and i_3 of the inverter and rectifier at P_n when the canceling windings are open or short. The validity of designing C_{s1} and C_{s2} with L_{eq} is confirmed because the power factor of v_{pri} and i_1 is unity. The DC output voltage V_{out} decreases as the equivalent mutual inductance decreases to $k_{eq}L_{eq}$.

Figure 10 shows the current i_m at K_{amp} = 1.00 and 1.30. The RMS current I_2 and I_4 are increased by 1.30 times with the additional power supplies.

E. Leakage Magnetic field

Figure 11 shows the fundamental component of H_z at the measurement point when K_{amp} changes from 0.75 to 1.33. The z-axis component H_z is measured with the magnetic probe (Electro-Metrics Corporation, EM-6993). Only H_z in the magnetic field is measured because H_z is dominant in H at the measurement point. The z-axis component H_z is 25.7 dBµA when the canceling windings are open. The fundamental

component of H_z is decreased by 39.5 dB at most with the proposed method. An error between K_{amp_z} and measurement K_{amp} of minimum H_z is 6.2% because of an increase in I_1 and I_3 for the proposed method. Figure 10 (b) shows that a 5.6% increase in I_1 and a 6.9% increase in I_3 with the proposed method. The ratio K_{amp} at minimum H_z is changed to cancel the increased magnetic field of the main windings.

F. *Variation of Electrical Characteristic*

Figure 12 shows the input/output power P_1 and P_3, and active power P_2 and P_4 of the canceling windings. The transmission power (P_3 - P_4) increases as K_{amp} becomes large. The increase in the transmission power should be given by decreasing in $k_{eq}L_{eq}$ with the proposed method because the transmission power is inverse proportion to the equivalent mutual inductance in the series-series compensated WPT system. In addition, the active power P_2 and P_4 of the canceling windings are much lower than the transmission power. Thus, it is verified that the main windings transmit power, and that the canceling windings cancels H with the proposed method.

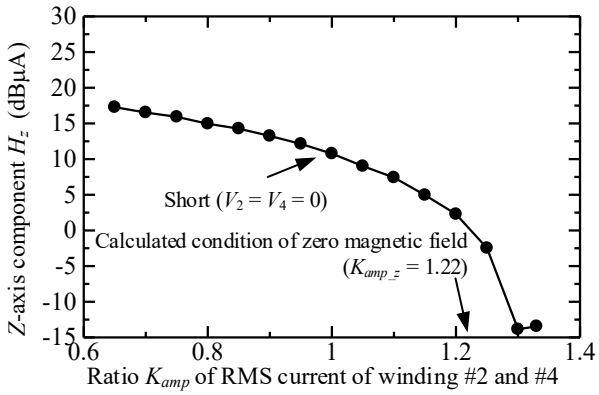

Fig. 11. Fundamental component of Magnetic field H_z.

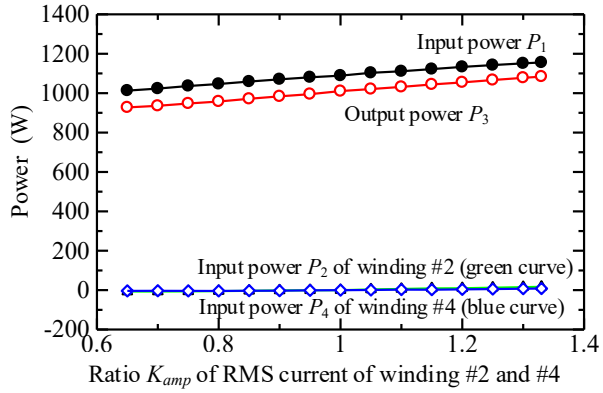

Fig. 12. Input/output power of each winding.

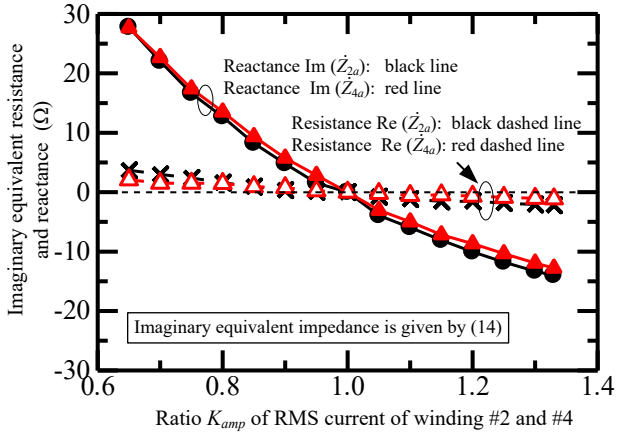

Fig. 13. Imaginary equivalent impedance $\dot{Z}_{2a}$ and $\dot{Z}_{4a}$ versus ratio K_{amp}.

Figure 13 shows the imaginary equivalent resistance Re ($\dot{Z}_{2a}$) and Re ($\dot{Z}_{4a}$) and reactance Im ($\dot{Z}_{2a}$) and Im ($\dot{Z}_{4a}$) of $\dot{Z}_{2a}$ and $\dot{Z}_{4a}$ versus K_{amp}. Note that Re ($\dot{Z}_{2a}$) and Re ($\dot{Z}_{4a}$) are negative when the bipolar power supplies are operated in generation mode. The imaginary equivalent impedance $\dot{Z}_{2a}$ and $\dot{Z}_{4a}$ are calculated with the measured $\dot{I}_m$, $\dot{V}_m$ and P_m of the canceling windings. The additional power supplies are operated as the capacitive load when K_{amp} is more than 1. The imaginary equivalent reactance Im ($\dot{Z}_{2a}$) and Im ($\dot{Z}_{4a}$) are much larger than Re ($\dot{Z}_{2a}$) and Re ($\dot{Z}_{4a}$).

Figure 14 shows the efficiency η versus K_{amp}. The efficiency η is given by

$$\eta = \frac{P_3 - P_4}{P_1 + P_2} \tag{16}.$$

Note that the canceling windings are connected to the bipolar power supplies at K_{amp} = 1.00 to compare η with the same circuit configuration. The efficiency η is decreased as K_{amp} increases. Thus, efficiency η is deteriorated by the injected reactance-compensated current to achieve the minimum H.

Figure 15 shows the estimated losses on the prototype of the WPT coils. The copper losses of the windings are calculated with measured RMS values of i_m and ESR in Table I. The iron loss is calculated with JMAG-Designer from measured $\dot{I}_m$. The copper losses of the main windings are dominant. The copper losses of the canceling windings are lower than the copper losses of the main windings by 7.7% at K_{amp} = 1.30. Thus, the copper loss of the main windings is clearly increased with the proposed method, although the increase in the copper losses of the canceling windings are negligible.

V. Conclusions

This paper proposed the low-radiation-noise WPT system with the injected reactance-compensation current as the active shielding. In addition, the changes of the electrical and magnetic characteristics are clarified when the proposed method is employed. The RMS current of the canceling windings is increased with the additional power supplies to inject the reactance-compensation current designed with the operation of rated power transmission when the canceling windings are short. The advantage is that the loss and capacity of the additional power supplies are smaller than those of the converters connected to the main windings. The experiment circuit parameters are designed with the equivalent self-inductance and

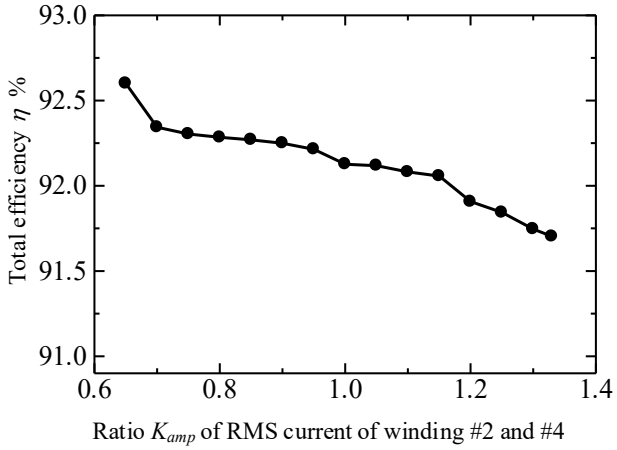

Fig. 14. Efficiency of overall WPT system.

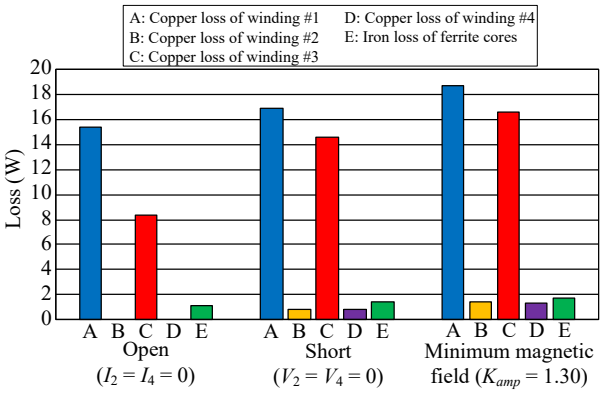

Fig. 15. Loss analysis of copper loss on each winding.

coupling coefficient of the prototype of the WPT coils when the canceling windings are short.

As a result, the transmission power of 1 kW and radiation-noise reduction of 39.5 dB are achieved with the proposed method. The calculated and measured RMS current of the lowest magnetic field agreed with the error of 6.2%. The transmission power of the WPT systems is increased as the decrease in the magnetic field with the injected reactance-compensation current. The efficiency of the WPT systems is deteriorated by the increase of the copper loss on the main windings due to the equivalent parameter variation of the WPT coils with the proposed method.

In the future, a current-compensation method will be evaluated when position misalignments of the WPT coils occur.

REFERENCES

[1] D. Patil, M. K. McDonough, J. M. Miller, B. Fahimi and P. T. Balsara, "Wireless Power Transfer for Vehicular Applications: Overview and Challenges", IEEE Transactions on Transportation Electrification, Vol. 4, No. 1, pp. 3-37 (2018)

[2] K. Kusaka and J. Itoh: "Development Trends of Inductive Power Transfer Systems Utilizing Electromagnetic Induction with Focus on Transmission Frequency and Transmission Power", IEEJ Journal of Industry Applications, Vol. 137, No. 5, pp. 328-339 (2017)

[3] G. Lovison, D. Kobayashi, M. Sato, T. Imura and Y. Hori: "Secondary-side-only Control for High Efficiency and Desired Power with Two Converters in Wireless Power Transfer Systems", IEEJ Journal of Industry Applications, Vol. 6, No. 6, pp. 473-481 (2017)

[4] H. Matsumoto, T. Zaitsu, R. Noborikawa, Y. Shibako and Y. Neba: "Control for Maximizing Efficiency of Three-Phase Wireless Power Transfer Systems At Misalignments", IEEJ Journal of Industry Applications, Vol.9, No.4, pp.401–407 (2020)

[5] International Commission on Non-Ionizing Radiation Protection (ICNIRP), "ICNIRP GUIDELINES FOR LIMITING EXPOSURE TO TIME-VARYING ELECTRIC AND MAGNETIC FIELDS (1HZ – 100 kHZ)", (2010)

[6] International Commission on Non-Ionizing Radiation Protection (ICNIRP), "ICNIRP GUIDELINES FOR LIMITING EXPOSURE TO ELECTROMAGNETIC FIELDS (100 kHz to 300 GHz)", (2020)

[7] Ministry of Internal Affairs and Communications, Japan, "Inquiry of technical requirements for wireless power transfer system for EVs in technical requirements for wireless power transfer system in standards of International Special Committee on Radio Interference (CISPR)", (2015)

[8] E. Asa, M. Mohammad, O. C. Onar, J. Pries, V. Galigekere and G. -J. Su: "Review of Safety and Exposure Limits of Electromagnetic Fields (EMF) in Wireless Electric Vehicle Charging (WEVC) Applications," 2020 IEEE Transportation Electrification Conference & Expo (ITEC), pp. 17-24 (2020)

[9] K. Inoue, K. Kusaka and J. Itoh: "Reduction in Radiation Noise Level for Inductive Power Transfer Systems using Spread Spectrum Techniques", IEEE Transactions on Power Electonics, Vol. 33, No. 4, pp. 3076-3085 (2018)

[10] K. Kusaka, K. Furukawa, and J. Itoh: "Development of Three-Phase Wireless Power Transfer System with Reduced Radiation Noise", IEEJ Journal of Industry Applications, Vol. 8, No. 4, pp. 600–607 (2019)

[11] I. Lee, N. Kim, I. Cho and I. Hong: "Design of a Patterned Soft Magnetic Structure to Reduce Magnetic Flux Leakage of Magnetic Induction Wireless Power Transfer Systems", IEEE Transactions on Electromagnetic Compatibility, Vol. 59, No. 6, pp. 1856-1863 (2017)

[12] H. Cui, W. Zhong, H. Li, F. He, M. Chen and D. Xu: "A Study on the Shielding for Wireless Charging Systems of Electric Vehicles", 2018 IEEE Applied Power Electronics Conference and Exposition (APEC), pp. 1336-1343 (2018)

[13] C. Lu, C. Rong, X. Huang, Z. Hu, X. Tao and S. Wang: "Investigation of Negative and Near-Zero Permeability Metamaterials for Increased Efficiency and Reduced Electromagnetic Field Leakage in a Wireless Power Transfer System", IEEE Transactions on Electromagnetic Compatibility, Vol. 61, No. 5, pp. 1438-1446 (2019)

[14] M. Lu, and K. D. T. Ngo: "Comparison of Passive Shields for Coils in Inductive Power Transfer", 2017 IEEE Applied Power Electronics Conference and Exposition (APEC), pp. 1419-1424 (2017)

[15] J. Park, D. Kim, K. Hwang, H. H. Park, S. I. Kwak, J. H. Kwon and S. Ahn: "A Resonant Reactive Shielding for Planar Wireless Power Transfer System in Smartphone Application", IEEE Transactions on Electromagnetic Compatibility, Vol. 59, No. 2, pp. 695-703 (2017)

[16] S. Y. Choi, B. W. Gu, S. W. Lee, W. Y. Lee, J. Huh, and C. T. Rim: "Generalized Active EMF Cancel Methods for Wireless Electric Vehicles", IEEE Transactions on Power Electronics, Vol. 29, No. 11, pp. 5770-5783 (2014)

[17] K. Furukawa, K. Kusaka, J. Itoh: "General Analytical Model of Inductance Variation by EMF-canceling Coil for Inductive Power Transfer System", IEEJ Journal of Industry Applications, Vol. 8, No. 4, pp. 660-668 (2019)

[18] S. Cruciani, T. Campi, F. Maradei and M. Feliziani: "Active Shielding Design for Wireless Power Transfer Systems", IEEE Transactions on Electromagnetic Compatibility, Vol. 61, No. 6, pp. 1953-1960 (2019)

[19] T. Campi, S. Cruciani, F. Maradei and M. Feliziani, "Magnetic Field Mitigation by Multicoil Active Shielding in Electric Vehicles Equipped With Wireless Power Charging System", in IEEE Transactions on Electromagnetic Compatibility, Vol. 62, No. 4, pp. 1398-1405 (2020)